Shape/penetration analysis and comparisons of isolated spray plumes in a multi-hole Diesel spray

N.B. When citing this work, cite the original published paper.

(article starts on next page)

Shape/penetration analysis and comparisons of isolated spray plumes in a multi-hole Diesel spray

Lokesh Mopuri[1] · Viljam Grahn[2] · David Sedarsky[1] · Jari Hyvönen[2]

Abstract

Fuel injection systems significantly impact the combustion process and play a key role in reducing harmful exhaust emissions in internal combustion engines. For dual-fuel (DF) engines operating in gas mode, ignition of the main fuel is typically controlled by directly injected liquid pilot fuel. Liquid pilot fuel's initial penetration and total mass considerably impact exhaust emissions and combustion stability. We investigated the spray morphology of a multi-hole diesel fuel injector within a constant-volume spray chamber using high-speed shadowgraphy and Mie-scattering measurements. Two methodologies were employed. The first one utilized a nozzle equipped with a thimble structure to isolate a single plume. The second methodology known as plume-blocking, involved sealing the orifices of the multi-hole nozzle to generate a single-spray plume. Our findings revealed that the plume-blocking approach demonstrated greater penetration than the thimble-equipped nozzle. The rapid penetration of this method may restrict its applicability to single-spray studies. Sprays generated from this partially sealed nozzle exhibited noticeable disparities compared to an unblocked nozzle, whereas a nozzle equipped with a thimble produced similar outcomes to the standard nozzle. The orifices when sealed, modify the flow distribution within the sac volume, which consequently affects the spray characteristics. In summary, this research provides insights into the impacts of various plume isolation methods on spray morphology, thereby enhancing the understanding of spray behaviour in transient conditions by comparing plume variations and disturbances under various fuel pressure and ambient conditions.

1 Introduction

Conventional diesel engines are highly valued for their compatibility, efficiency, dependability, and cost-effectiveness and energy density. However, they emit oxides of nitrogen

Viljam Grahn, David Sedarsky and Jari Hyvönen have contributed equally to this work.

✉ Lokesh Mopuri
mopuri@chalmers.se

Viljam Grahn
viljam.grahn@wartsila.com

David Sedarsky
sedarsky@chalmers.se

Jari Hyvönen
jari.hyvonen@wartsila.com

[1] Division of Energy Conversion and Propulsion Systems, Chalmers University of Technology, 41296 Gothenburg, Sweden

[2] Research & Technology Development, Marine Power Solutions, Wärtsilä Finland Oy, 65100 Vaasa, Finland

(NO_x) and particulate matter (PM), which are detrimental to human life and the environment (Okajima and Kumagai 1991). To reduce these emissions, stricter regulations are being implemented. Alternative fuels are recognized as a potential solution to reduce greenhouse gas emissions and address the challenge of balancing energy demands with dwindling oil reserves (Agarwal et al 2015). In this context, natural gas is gaining attention as a promising and viable alternative energy source for conventional diesel engines (Srinivasan et al 2014), which is also affordable and available worldwide (Wei and Geng 2016). Today, natural gas is widely seen as one of the potential transition fuels that could help bridge the gap until clean, carbon-free, and green e-fuels become more readily available in larger quantities. In dual-fuel (DF) compression ignition (CI) engines, natural gas (CNG) exhibits poor ignition characteristics due to its lower cetane number and a higher auto-ignition temperature compared to diesel fuel (Chandra et al 2011). Therefore, an ignition source is always necessary to ignite the natural gas in the cylinder. The gas is introduced into the cylinder through the intake valve during the intake stroke, and a small quantity of high-cetane fuel (diesel) is injected into

the combustion chamber near the top-dead centre to ignite the lean air–gas mixture. To achieve low NO_x emissions, injected fuel must be minimal. Typically, injecting less than 5% diesel fuel (Wärtsilä Corporation 2023) at nominal load results in NO_x emissions approximately one-tenth of a standard diesel engine (Sombatwong et al 2013). Moreover, to avoid knocking and misfiring while operating DF engines in gas mode, the timing and quantity of micro-pilot injection must be precisely controlled to keep each cylinder at its optimal operating point (Pounder and Woodyard 2004).

Therefore, gaining a deeper understanding of pilot spray atomization and its transient behaviour is crucial in ensuring optimal performance of DF engines, where fuel mixture formation is a critical aspect that significantly affects engine performance and emissions. To study this process, researchers have employed various injector modifications, such as single-hole and multi-hole configurations, to facilitate spray analysis. For instance, Payri et al (2016) utilized custom-made single-hole injectors, whereas (Pal and Bakshi 2017; Baert et al 2009) employed micro-welding techniques to modify multi-hole nozzles into single-hole configurations. These studies then investigated the sprays in high-pressure, high-temperature chambers (Baert et al 2009; Pickett et al 2022; Payri et al 2014; Deshmukh 2011) using various visualization methods. The spray behaviour of multi-hole nozzles differs significantly from that of single-hole nozzles (Shi et al 2011). Moon et al (2015) demonstrated that multi-hole nozzles exhibit faster spray breakup and deceleration of the axial velocity compared to single-hole nozzles with axisymmetric holes. Similar to a single-hole nozzle, blocking all but one hole in a multi-hole nozzle results in accelerated pressure buildup within the nozzle sac. This phenomenon, in turn, promotes faster needle lift. Consequently, the final pressure within the system increases due to the amplified momentum flux associated with the reduced flow area Baert et al (2009). Additionally, He et al (2013) highlights the crucial role of orifice hole placement in controlling the flow within the sac volume. (Jin et al 2020) reported that single-hole nozzle injectors achieve deeper spray penetration than multi-hole injectors under the same injection pressure conditions. However, this enhanced penetration is likely to come at the cost of a slower evaporation rate due to the dense liquid core and less effective mixture formation compared to multi-hole injectors. These findings suggest that using single-hole nozzles significantly alters the injection process, resulting in trade-offs between spray characteristics and mixing efficiency.

Despite this, single-hole (SH) injectors remain popular in spray studies due to their inherent ease of use. This characteristic allows researchers to readily grasp fundamental spray behaviour and easily apply optical diagnostic tools around the single-spray plume. However, the majority of diesel engines rely on multi-hole (MH) injectors (Jin et al 2020) to achieve sufficient fuel flow through the orifice holes. These nozzles strategically position the holes around the nozzle axis, typically in a symmetrical arrangement. Compared to an axisymmetric single-hole injector, this off-axis design generates significantly more complex internal and external flow patterns (Moon et al 2015). Despite this complexity, many engine combustion simulations draw upon spray models derived from single-hole injectors. Therefore, understanding the fuel spray and flow characteristics of both injector types is crucial for bridging the gap between theoretical models and the actual behaviour of engines. This comparison is even more critical for pilot sprays due to their transient nature.

Pilot sprays are small amounts of fuel that are injected at low needle lift conditions, which makes them highly sensitive to injector transitional behaviour. Understanding the characteristics of these transient sprays is crucial for optimizing direct pilot fuel ignition and combustion. The investigation of these pilot sprays using optical diagnostics,
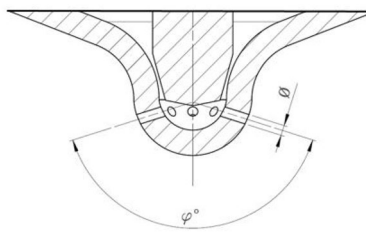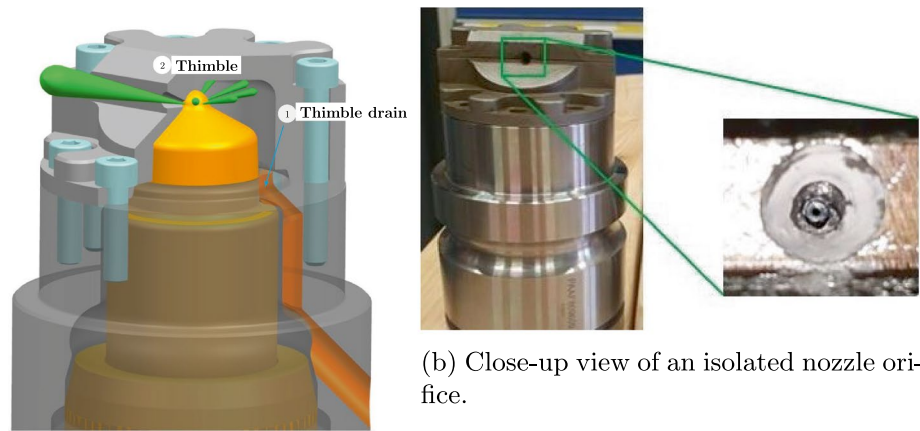
Table 1 Nozzle parameters

Nozzle with 9-Orifices	Parameters	Value/Units
	Number of holes	9
	Hole diameter (∅)	0.31 mm
	Umbrella angle ($\varphi°$)	145 degree

Fig. 1 Schematic view of plume isolation methods

(a) Schematic of thimble design (not to scale).

(b) Close-up view of an isolated nozzle orifice.

(c) Sealed (micro-welding) nozzle.
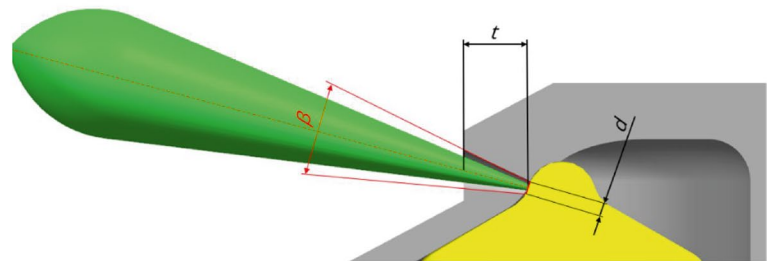
(d) Thimble hole dimensions.

particularly without any injector modifications, is significantly limited in existing spray studies. Hence, in order to avoid modifications to the injector nozzle that might alter spray characteristics, the study introduced the concept of a thimble (Klein-Douwel et al 2007), which is a cap-like structure located above the injector nozzle. This thimble isolates the single-spray plume from the spray generated by the multi-hole nozzle. This study aims to achieve two primary objectives: firstly, to introduce spray isolation methods, and secondly, to analyse and compare the spray morphologies of isolated spray plumes and multi-plume sprays, including their deviations. To isolate the single-spray plume, the study employed two concepts: a thimble and blocking the nozzle holes. The resulting sprays from these concepts are referred to as plume-thimble and plume-blocking, respectively. The multi-plume spray from a multi-hole nozzle is referred to as plume1–9.

2 Materials and methods

This section details the spray test rig, fuel delivery system, test matrix, optical set-up, and methodologies for isolating spray plumes in multi-hole diesel sprays and the image processing methods employed to extract spray data.

2.1 Nozzles and injection system

The fuel delivery system is crucial for delivering fuel at the appropriate pressure and rate. This system comprises two main components: a hydraulic fuel pressure amplifier and a fuel supply line. The fuel supply line has an electronic pressure regulator and pressure sensor that regulate the injection pressure. During each 10-s pressurization cycle, the fuel pressure is determined by the hydraulic pressure available in the system, which is then supplied to the injector. A marine diesel injector with a nine-orifice nozzle was used for the

Table 2 Test matrix

Nozzle set-up	Multi-hole, blocked nozzle, and thimble method
Test matrix conditions and nozzle set-up	
Chamber inside densities (kg/m^3)	14.62, 27.69
Corresponding ambient pressures (bar)	12.30, 23.30
Fuel pressures (MPa)	170, 210
Injection duration (μs)	500
Ambient gas	Air
Ambient temperature (K)	≈ 300

Table 3 LFO properties (Wärtsilä Corporation 2023)

Property	Value	Unit
Density @ 15 °C	833.5	kg/m^3
Viscosity @ 40 °C	3.036	mm^2/s
Flash point	64.5	°C
Sulphur (Low level)	< 10	mg/kg

experiments, and the nozzle parameters are listed in Table 1. The nozzle orifices are cylindrical in shape with a typical K-factor of zero. The injector was maintained at around 300 K to ensure consistent testing conditions, as all laboratory investigations were conducted at room temperature. In the experiments, a commercial light fuel oil (LFO) with a density of 833.5 kg/m^3 (at 15 °C) and a kinematic viscosity of 3.036 mm^2/s (at 40 °C) was used as fuel.

2.2 Strategies for isolating spray plumes

The thimble hole has a conical shape that diverges outward. We gradually modified the thimble to ensure that the dimensions were appropriately sized to prevent any interference with the spray. These set points were determined based on observations in which no apparent plume deviation was observed. Specifically, the cone's apex (d) is designed to be at least twice the size of the orifice hole. The cone angle in the thimble should be greater than the cone angle of the spray to prevent interference with the thimble wall surface. Ideally, the thimble angle (β) should be 1.5 times greater than the widest cone angle observed in the spray. In our current experiments, this angle (β) is approximately 55 degrees, while the thimble thickness (t) is set to 4.7 mm. Figure 1d illustrates these dimensions.

To examine a single-spray plume, isolating it from the multi-plume produced by the multi-hole nozzle is necessary to avoid optical interference. This study employed two methods to achieve this isolation. The first method involved blocking or sealing all other nozzle holes except for the one being utilized (see Fig. 1c); the resulting spray plume is referred to as plume-blocking. The second method involved constructing a thimble that was attached to the nozzle, as shown in Fig. 1a. With this method, only one spray plume (plume-thimble) could be injected into the chamber, while all other plumes were collected and drained. The injector was positioned at an incline at the bottom of the chamber, as depicted in Fig. 3. Therefore, the collected fuel flowed directly into the chamber's drain. Furthermore, the timing

of the thimble drain valves was precisely controlled after each injection cycle to prevent an increase in ejected fuel pressure in the drain passages or the thimble itself. The spray plume produced by the ninth hole was chosen for the thimble method, so the ninth plume (plume9) was directly injected into the chamber while the thimble collected the remaining plumes.

The initial set-up used a thimble thickness of 4.7 mm and a relatively small angle of approximately 45 degrees (β). However, this small angle caused interference within the spray plume. To address this issue, we adopted an iterative approach. At each stage, we gradually increased the angle while simultaneously applying white paint to the inner thimble surface (see Fig. 1c). Following each grinding and painting stage, we conducted spray experiments and visually inspected the thimble surface for any paint removal by the spray. This process continued until the paint remained unaffected, suggesting a suitable thimble angle. Notably, this angle was chosen to be almost 1.5 times the largest spray cone angle observed in our experiments, effectively eliminating interference. The results presented in this paper are based on experiments conducted with a thimble thickness of 4.7 mm. In later experiments, we aimed to reduce the thimble thickness from 4.7 mm to improve the visibility of the spray near the nozzle. We eventually minimized the thickness to 2.6 mm. A larger thickness was not recommended as it obscured the initial spray.

2.3 Test matrix

A range of diverse test conditions were chosen to gain insight into spray characteristics. Test conditions were carefully selected to investigate the pilot spray's complete behaviour. The experiment involved the examination of specific test points, detailed in Table 2. These chosen conditions aimed to replicate the thermodynamic aspects pertinent to large bore engines while also shedding light on how these pilot sprays affect engine performance in transient scenarios of LFO (Table 3).

2.4 Constant-volume spray test rig

Constant-volume chambers are commonly used for spray observation because their large size and minimal

Table 4 Characteristics of OSCC

Parameter	Value
Outer dimensions	$600 \times 600 \times 550$ mm
Volume	0.0172 m^3 (17.2 l)
Pressure	0–400 bar
Temperature	20–200 °C
Operation modes	
Cold	Nonreactive sprays
Hot	Reactive sprays
Heat and pressure generation	
Cold	Pressurized air
Hot	Pre-combustion

obstructions ensure a clear and extensive visual field, and reproducibility of the thermodynamic conditions prior to the injection (Payri et al 2013a). Spray testing was conducted in the Wärtsilä's Optical Spray Combustion Chamber (OSCC) located in Vaasa, Finland. It is a constant-volume pre-combustion hot cell test rig, which is designed to operate in the same manner as Baert et al (2009) and is suitable for testing large bore medium speed marine engine injectors. Table 4 depicts the characteristics of the chamber.

The chamber is cubical and equipped with several modules, including a gas exchange system, an injector adapter, and optical windows. The spray can be observed through any

of the four windows available, depending on experimental requirements. The injector is mounted upside-down beneath the chamber body, while the hydraulic gas exchange valves, exhaust pipes, and gas lines are placed at the back of the chamber. To maintain consistent experimental conditions, the chamber was emptied and refilled using exhaust and inlet valves after every five sprays, thus minimizing the potential for fuel mist interference on the primary spray structure.

2.5 Optical set-up

The current investigation employed two imaging techniques for observing sprays: the Mie-scattering method for observing a multi-spray and the back-lighting method for observing a single spray, i.e. plume-blocking and plume-thimble. The LED (constellation 120E manufactured by Veritas) lights are mounted on each side of the spray chamber to provide volumetric illumination of the plumes during Mie-scattering. As shown in Fig. 2, the injector is positioned vertically at the bottom of the chamber, and the images were captured from the top plane. The light source and imaging devices are synchronized so that the light intensity is automatically adjusted and maintained at a constant level based on the frame rate and exposure time.

Back-lighting is another illumination method that was used in this study. It is commonly used for spray liquid phase measurements and visualization experiments. In this method,

Fig. 2 Schematic representation of Mie-scattering optical configuration
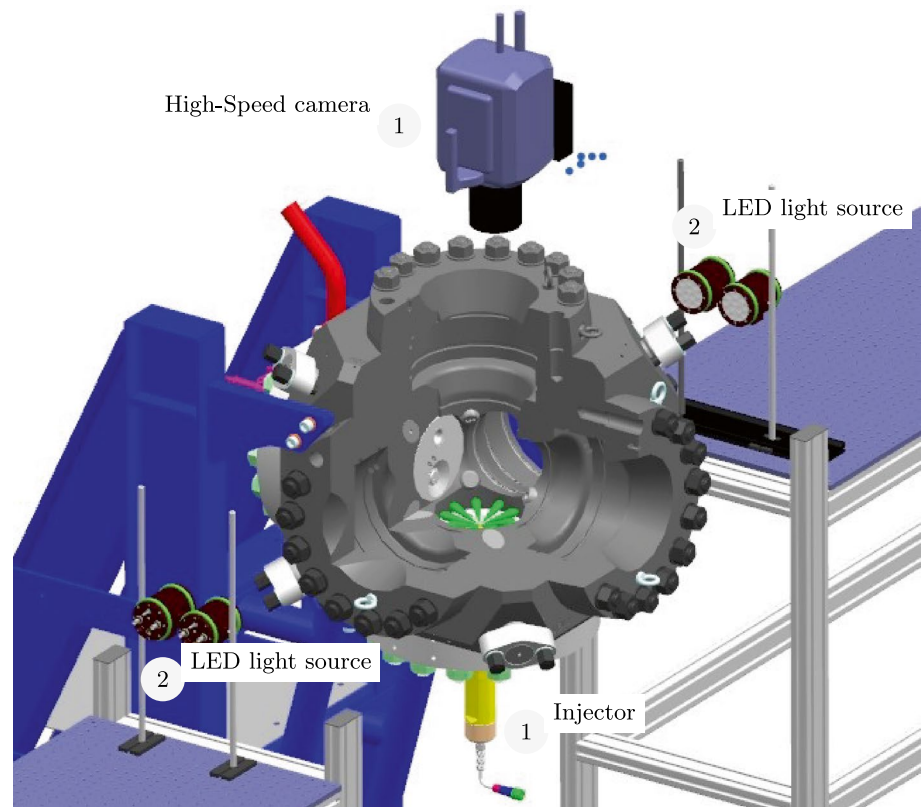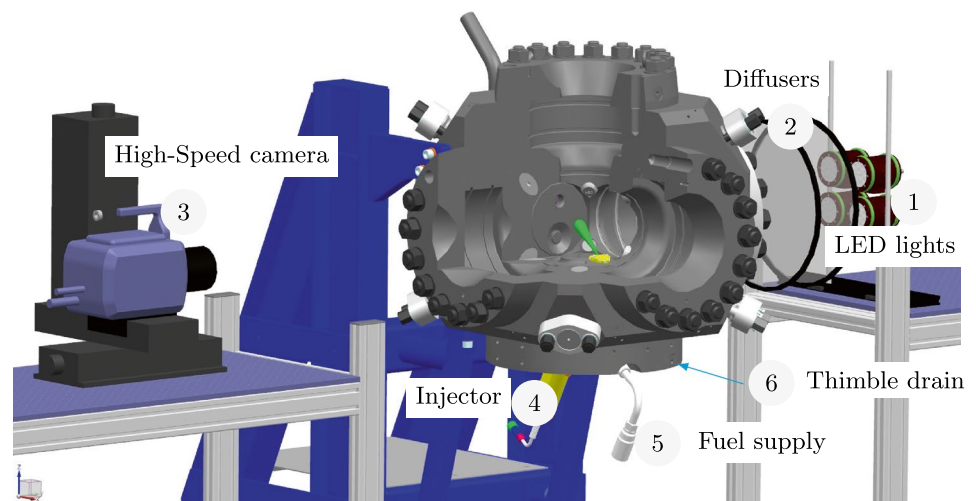
Fig. 3 Schematic representation of Diffuse backlight configuration

the light source and imaging device are positioned opposite to one other and oriented in the same direction, as shown in Fig. 3. Both experiments used a CMOS high-speed camera equipped with a Micro NIKKOR lens to capture the spray events. The lens has a 105-mm reach, a maximum aperture of f/2.8, and a 1:1 reproduction ratio, producing clear and detailed spray images. The images acquired at 35,000 frames per second with 512×512 pixels resolution and 9 and 3 ms exposure times were selected in Mie-scattering and back-light imaging, respectively.

2.6 Image post-processing procedures

This study applied image processing and contour recognition techniques to digital photographs using in-house code written in MATLAB. An image captured before injection was subtracted from the spray image to eliminate reflections and background artefacts. This subtracted image was then converted into a binary image using Otsu's algorithm (Otsu 1979) for automated thresholding. Next, a masking technique (Pastor et al 2007; Macian et al 2012; Payri et al 2013c) was employed to divide the multi-plume spray image into distinct sections corresponding to each plume, allowing for an independent plume analysis. The central axis angle of each plume was calculated with respect to the horizontal line, and the plumes were subsequently rotated to a vertical orientation for ease of coding. In the final step, the penetration length, surface area, and spray cone angles were determined for each plume. To analyse the spray characteristics of images captured with back-light, we applied the same procedure of generating a binary vertical image to both plume-blocking and plume-thimble images. Subsequently, a thorough analysis was conducted on the resulting images to examine the spray characteristics.

2.6.1 Spray penetration length (S)

The spray penetration length is the farthest distance the spray reaches when injected into the air, defined as the distance from the tip of the nozzle to the farthest axial location of the spray. However, this method of direct calculation may not be consistent because some outlier droplets, which are not part of the main spray, may also be detected. Including these outliers in the penetration length measurement introduces errors. To reduce these errors, in the present study, the penetration length is defined as the distance from the nozzle tip (along the spray axis) to a downstream point where most of the spray droplets are confined, specifically the length that covers 99% of the projected spray area (Pal and Bakshi 2018).

2.6.2 Spray area (SA)

In the spray binarized image, the spray area is calculated by summing all pixels with one value. Due to the missing information, an equivalent area of the spray was added to
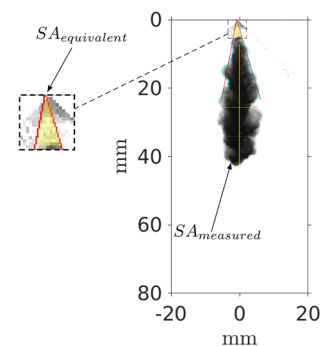

Fig. 4 Spray area hidden by thimble thickness

the measured spray area (SA(mm^2) = Area (pixels^2)× (mm/pixels)^2) for the plume-thimble (see Fig. 4).

2.6.3 Spray cone angle (θ)

One of the most common ways to calculate the spray cone angle is by using the angle formed by two lines fitted to the spray boundary edges. A least-square fit determines which lines best fit the spray edges. These lines can be either near or far-field, with distances proportional to the spray penetration length or multiples of the nozzle orifice diameter (D). Ideally, these lines could be extended to the nozzle tip coordinates, where they may or may not intersect, resulting in different cone angles calculated in each case. In the present study, the cone angle was determined as follows: as a first step, the spray contour was detected using binarisation and a guess-fit line was drawn inside the spray contour by fixing the line origin at the spray origin (see Fig. 5c). The line moves towards the one side spray edge, and the least-square error was calculated at each move (at each pixel position). This continues until the least square value reaches

a minimum, as shown in Fig. 5c. Similarly, the same procedure was applied to identify the fit line on the other side spray edge, and the angle calculated between these lines can then be referred to as the cone angle for that specific spray. The thimble used here conceals the initial spray up to 4.7 mm (thimble thickness). Because of this, it is unable to utilize the spray boundary within the thimble when calculating least squares. However, the spray contour was positioned between the thimble exit, and 60% of the spray penetration length was selected to compute the least square error. To maintain consistency in measurement methods and avoid the variance in cone angles that may arise from the use of different approaches, spray below 4.7 mm from the nozzle tip is excluded from the calculation of cone angles for plume-blocking and multi-plume sprays (plume1–9). In all case, the fit lines were drawn from a virtually fixed spray origin (see Fig. 5) which is identical to the nozzle tip (Fig. 6).

Spray visualizations have been conducted from a front view of the multi-hole nozzle, with orifice holes evenly positioned at a 40-degree angle, while the spray plumes are directed 17.5 degrees away from the injector plane. Thus,

Fig. 5 A schematic diagram for measuring spray penetration and cone angle

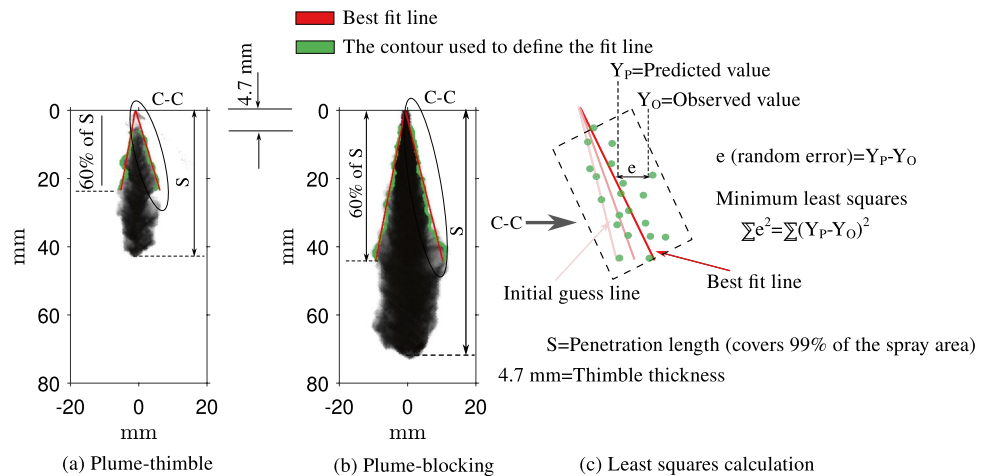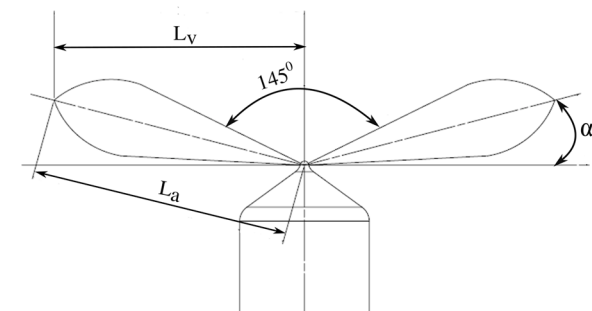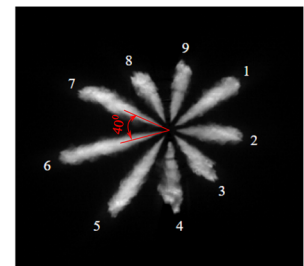(a) Plume-thimble　　　(b) Plume-blocking　　　(c) Least squares calculation

Fig. 6 Calculation of the actual penetration length (L_a)

(a) Side view of the multi-hole (MH) injector spray (not to scale).

(b) Front view of the multi-hole (MH) injector spray and plume numbering. Test conditions: $\rho_{amb} = 14.62 \, \text{kg/m}^3$, $P_{inj} = 210$ MPa.

the approximate penetration length (L_a), which is close to the actual value, was calculated from the visually observed penetration length (L_v) using the equation $L_a = \frac{L_v}{\cos \alpha}$, where $\alpha = 17.5°$ represents the angle between the actual and measured penetration length axis.

3 Results and discussion

The report is structured into three parts to present the results and analysis. In the initial segment, the analysis focuses on the influence of ambient density on spray characteristics and includes a comparison between plume-blocking, plume-thimble, and plume9 extracted from a multi-plume spray. The selection of plume9 was intended, as it was generated using a nozzle fitted with a thimble; consequently, only data related to plume9 is presented in this section. The second part provides a summary of the effects of fuel pressure on the spray in all three cases discussed in the first part. Finally, the third part compares the variations among the multi-plume (plume1–9) and contrasts them with the results obtained from the comparison between plume-blocking and plume-thimble. The spray characteristics, encompassing spray penetration (S), spray area (SA), and spray cone angle (θ) for each spray image captured during the injection

event, are directly measured. The results presented in the following graphs reflect an average of fifteen spray events, with repeatability bands depicted as shaded areas around the penetration, spray area, and angle data points. The start of injection time (SOI) is determined directly from the first image showing detectable fuel in experiments involving multi-plume as well as plume-blocking. When using the thimble, however, this method cannot be used, since the thimble blocks the spray at its beginning. To maintain consistency and accuracy in our study, we computed the hydraulic delay from the direct multi-hole visualization experiments. Subsequently, we applied the same hydraulic delay to the plume-thimble spray to estimate the SOI. In all experiments conducted, consistency was maintained by utilizing the same injector and nozzle configuration, regardless of whether investigating the multi-hole spray, applying the thimble method, or utilizing the sealed nozzle. Initially, emphasis was placed on testing the multi-hole nozzle to analyse the multi-plume spray. Subsequently, the thimble method was introduced to isolate and study a single-spray plume. In the final stage of experimentation, the same nozzle was sealed to produce a single spray. Although both Mie-scattering (multi-plume) and back-lighting (single-spray) techniques were employed in our experimental set-up, their uncertainties encompass multiple scattering in

Fig. 7 Influence of ambient density on spray characteristics: penetration length, spray area, and cone angle
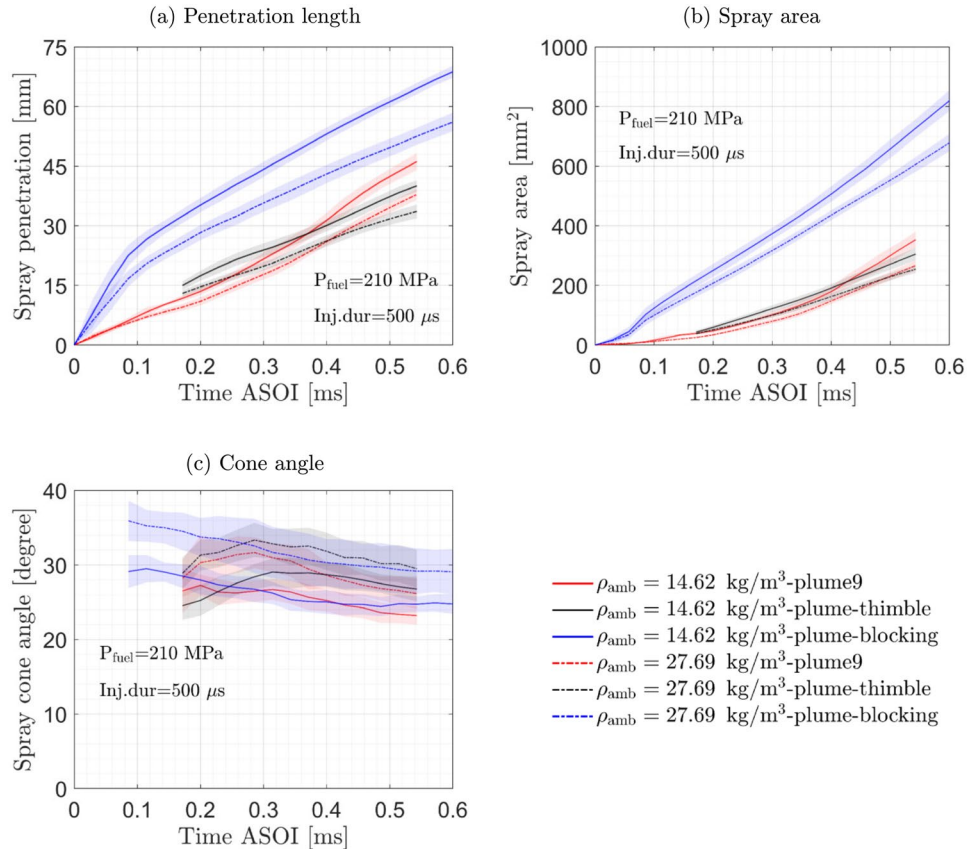
Mie-scattering and beam steering in back-lighting. These uncertainties, however, are likely to have a minimal impact on the comparison between the two imaging methods in current experiments. This is because vapour generation observed at ambient temperatures is minimal.

3.1 Comparison of plume-thimble, plume-blocking, plume9

Figure 7 illustrates the spray characteristics, such as penetration length, spray area, and cone angles, of three distinct plume configurations: plume-blocking, plume-thimble, and plume9. The results are compared at various ambient densities while maintaining a constant fuel pressure of 210 MPa (P_{inj}), and the electrical control signal duration (Inj.dur) is 500 µ. For comparison purposes, two ambient densities are considered, such as $\rho_{amb} = 14.62$ kg/m^3 and $\rho_{amb} = 27.69$ kg/m^3. From Fig. 7a, it was confirmed that the plume-blocking penetrates faster than the plume-thimble. For example, at 0.4 ms ASOI, the plume-blocking penetration length was nearly 1.5 times greater than that of the plume-thimble under both ambient densities.

This indicates that the blocking strategy alters the injection process. In the study by Baert et al (2009), blocking the holes accelerated the nozzle sac's pressure buildup, which led to a quicker needle lift and higher pressure readings at full needle lift. Furthermore, the images also reveal that the plume-blocking penetration length is substantially higher than plume-thimble as shown in Fig. 8 at 14.62 kg/m^3(ρ_{amb}), as well as in Fig. 9 at 27.69 kg/m^3(ρ_{amb}). It can also be observed that as the ambient density increases, both the penetration length (Fig. 7a) and spray area (Fig. 7b)
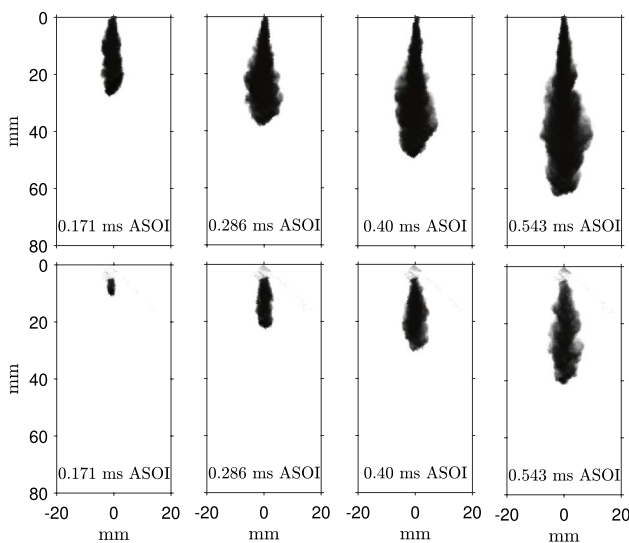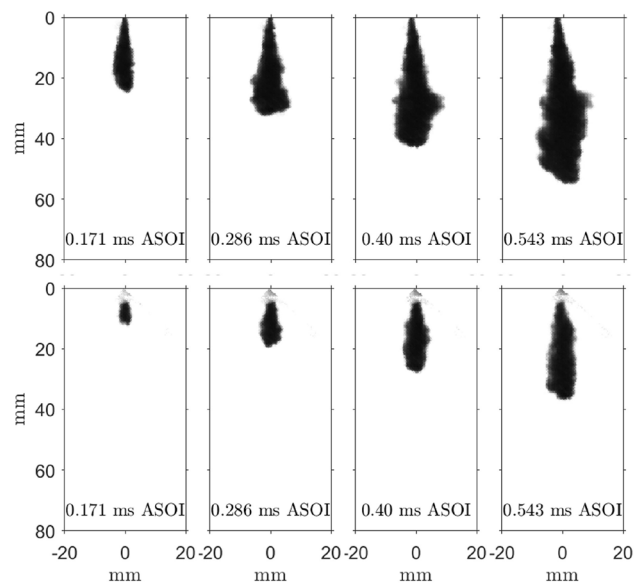
Fig. 9 Image sequences of plume-blocking (first row), plume-thimble (second row) at $\rho_{amb} = 27.69$ kg/m^3, $P_{inj} = 210$ MPa

decrease, while the cone angle (Fig. 7c) increases. This is because, changes in ambient density would primarily affect air entrainment and momentum exchange. So, increase in ambient density could alter the vapour pressure gradient between the droplet surface and the surrounding air. When the density of the gas surrounding a spray is higher, there are more gas molecules in a given volume. As the spray moves through this denser gas, it encounters more resistance because there are more molecules that it needs to push aside to make its way through. To overcome this resistance and penetrate deeper into the surrounding gas, the spray needs more kinetic energy, thus spray penetrates slower (Payri et al 2013b).

When comparing the plume-thimble with plume9, both show similar penetration lengths, as illustrated in Fig. 7a. For example, at an ambient density of $\rho_{amb} = 14.62$ kg/m^3, and also at higher ambient density ($\rho_{amb} = 27.69$ kg/m^3), the similar behaviour is observed. However, the plume9 shows a sudden uptick near 0.4 ms ASOI, which is visible on both penetration (Fig. 7a) and area graphs (Fig. 7b) while the plume-thimble trend remains steady without any noticeable spikes. This might be due to the thimble, air entrainment would decrease due to the thimble that prevents fluctuations in the spray pattern, which, in turn, makes spray penetration and area patterns more consistent. Despite these observations, the cause of this difference is unclear and requires further investigation. The utilization of different optical imaging methods also introduces some error into the results. Specifically, the back-light imaging technique was employed to capture the plume-thimble spray, while Mie-scattering was used to visualize the multi-plume spray. The

Fig. 8 Image sequences of plume-blocking (first row) and plume-thimble (second row) at $\rho_{amb} = 14.62$ kg/m^3, $P_{inj} = 210$ MPa

nearby walls of the chamber will have a subtle effect on the sprays (Leick and Bartole 2023), but it is important to note that the wall effects in our current experiments are likely minimal. This is because the volume of the spray chamber is significantly larger, around 17.2 ls. As a result, the transient spray (pilot spray) does not reach the chamber walls.

Light reflections from the chamber surface walls, particularly the adapter surface, significantly hampered the accurate detection of the spray contour. To mitigate this issue, the faces of the injector adapter were coated with black paint to reduce light reflections. However, the difference exists in cone angle values between Mie-scattering (plume9) and back-light imaging (plume-thimble). Figure 7c demonstrates that cone angles obtained via Mie-scattering were smaller than those acquired through back-light imaging. The intensity of Mie-scattering signals depends on droplet size, particularly because the outer edges of the spray contain very small droplets. Therefore, cone angles are influenced by light intensity. As the diagram illustrates, even at ambient densities, cone angles appear to be higher for back-light imaging. The periphery of the spray boundary consists of small droplets that scatter less intense light, which the high-speed camera sensor may not capture. Additionally, droplets with lower intensity are potentially excluded during the image segmentation process, directly impacting cone angle measurements since

these measurements are based solely on the spray boundary. These variations are minimal when comparing the results of spray penetration and spray area between back-light and Mie-scattering technique (see Fig. 7a, b). Analyses exhibited maximum standard deviations of ± 1.8, ± 15, and ± 2.8 for penetration length, area, and cone angle, respectively, across all experiments.

3.2 Influence of the injection pressure

Figure 10 illustrates how spray characteristics may vary with injection pressure when the ambient density is constant. In the case of plume9 and plume-thimble, the injection pressure is less influential on spray characteristics, and there is no noticeable difference in spray area and cone angle. But, a noticeable difference is observed in the case of the plume-blocking; this also indicates that the blocking approach modifies the flow distribution inside the sac volume. The ambient gas density significantly influences air entrainment. Higher ambient densities lead to increased air entrainment into the spray, particularly for the pilot spray due to the small amount of fuel involved and its weaker liquid core, which enhances atomization and mixing. Due to this, shorter penetration lengths are observed with increasing ambient densities. While increasing the fuel injection pressure primarily affects the initial spray velocity, with a

Fig. 10 Influence of fuel pressure on spray characteristics: penetration length, spray area, and cone angle
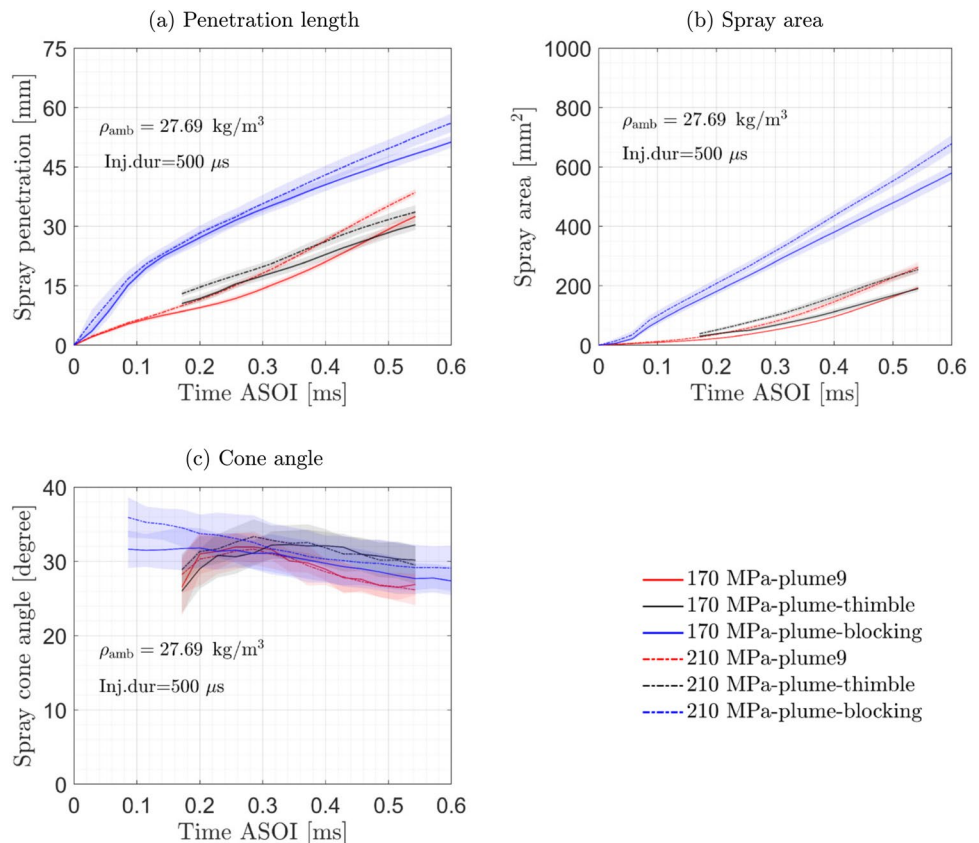
lesser impact on air entrainment. However, while increasing injection pressure definitely influences spray penetration, area, and cone angles, in these experiments, the fuel pressure was increased by only around 24%, so the influence is not as noticeable compared to the increase in ambient density, which was almost doubled.

3.3 Plume to plume deviation

The injector with a multi-hole nozzle injects fuel at varying rates, which significantly impacts the combustion characteristics of diesel engines, resulting in increased pollution and inconsistent thermal loads (Luo et al 2014). In order to gain a better understanding of plume deviations, the current research investigates the multi-plume spray thoroughly using the Mie-scattering technique. This section compares the degree of variation between multi-plume spray (plume1–9), plume-thimble, and plume-blocking sprays. The test points

used in this multi-plume spray study are the same as those used in a thimble and blocking methods. The spray penetration length, area, and cone angles were normalized with their respective maximum values across all the plumes (see Figs. 11, 13 and 14).

The plumes have significant variations in penetration at low ($\rho_{amb} = 14.62$ kg/m^3) and high ($\rho_{amb} = 27.69$ kg/m^3) ambient densities, as shown in Fig. 11. Furthermore, variations in the early stages of the injection process can be observed (Fig. 11a), but these variations disappear over time (Fig. 11d). These variations are also apparent in the spray image sequence, as shown in Fig. 12. The variations in the injection process between holes can be attributed to a lack of precision in manufacturing processes (Pal and Bhagwat 2015) and lateral needle oscillations (Battistoni et al 2014). According to Wang et al (2018), the nozzle hole closest to the needle displacement has a much higher degree of obstruction from the needle tip. In contrast, the nozzle

Fig. 11 Comparison of penetration for multi-plume and single plume (blocked nozzle and thimble connections) at different ambient densities
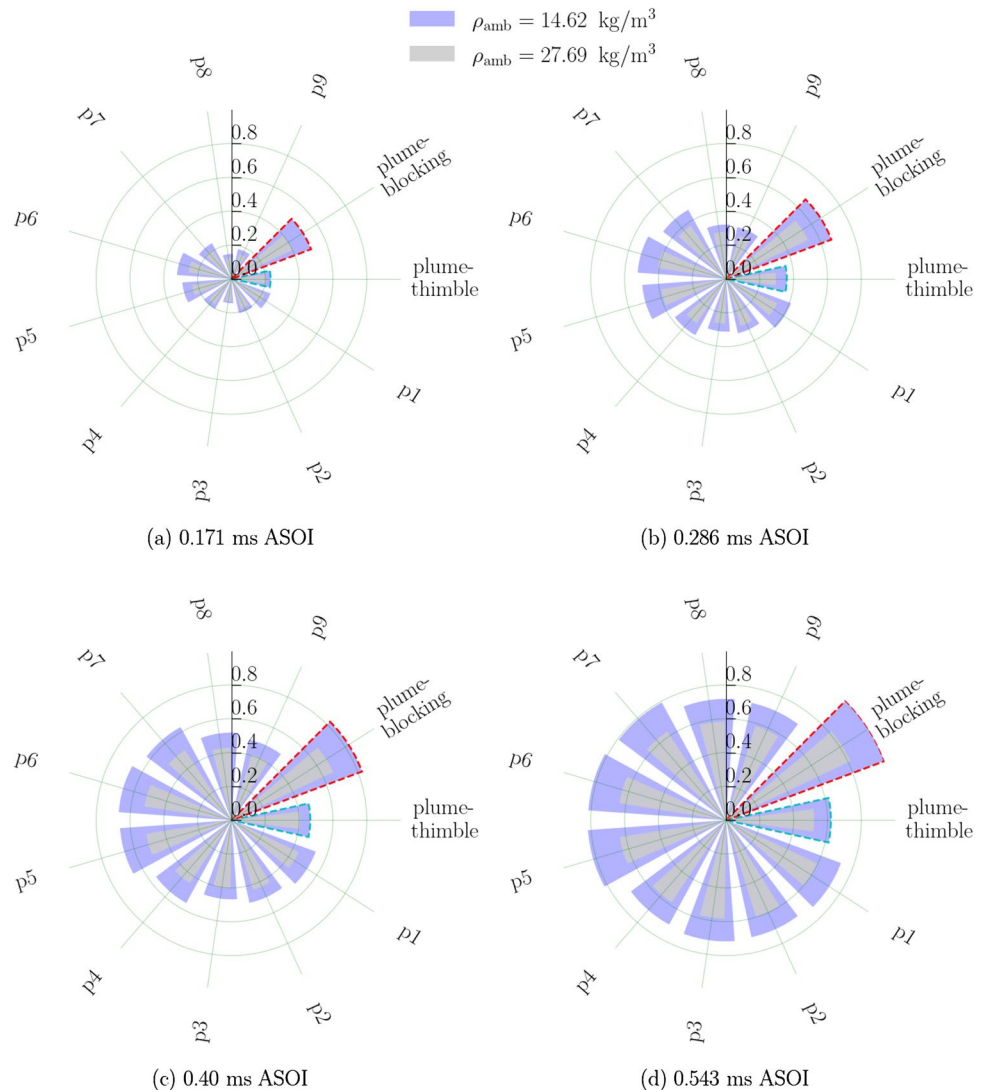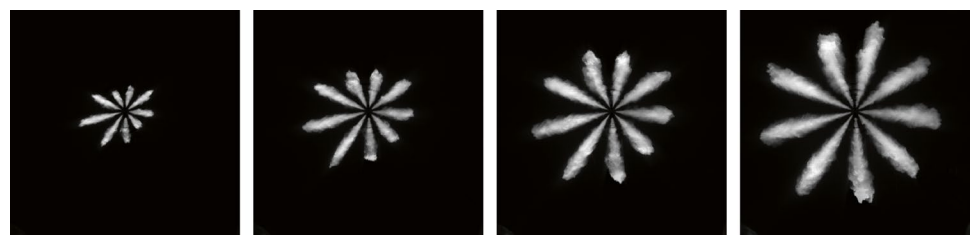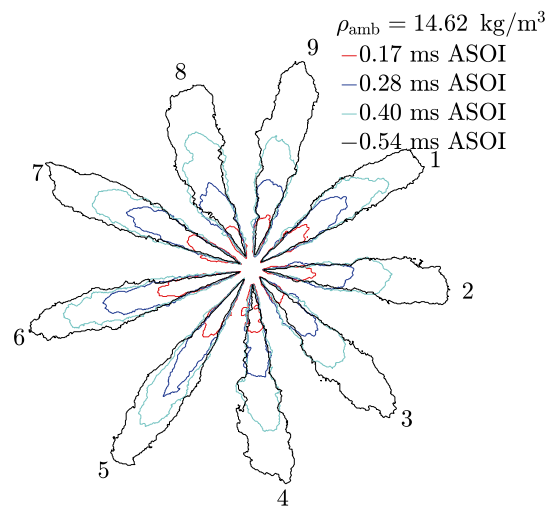
(a) 0.171 ms ASOI

(b) 0.286 ms ASOI

(c) 0.40 ms ASOI

(d) 0.543 ms ASOI

Fig. 12 Image sequences of multi-plume at $\rho_{amb} = 14.62$ kg/m^3, $P_{inj} = 210$ MPa, $T_{amb} = 300\,K$

(a) 0.171 ms ASOI   (b) 0.286 ms ASOI   (c) 0.40 ms ASOI   (d) 0.543 ms ASOI


(e) Spray contours

hole farthest from the needle displacement has a relatively reduced interference from the needle tip, giving it a greater geometric flow area. The effect of transient needle movement on flow distribution inside nozzle holes is therefore reflected in the absence of homogeneity during the fuel injection process.

The pattern of penetration lengths for plume9 and plume-thimble is similar, with only a negligible difference. These differences can be attributed to experimental errors between the two imaging techniques. The ninth hole was chosen for analysis with a thimble as it produces one of the weakest plumes among the nine plumes, as shown in Fig. 12a–c and 12e. This allows for determining the maximum plume deviation between plume-thimble and plume-blocking. However, the results show that the plume-blocking had greater penetration than all other plumes (plumes1–9), making the choice of specific holes for investigating single sprays with a thimble less relevant as the plume-blocking approach penetrates more rapidly than most plumes.

Figure 13 illustrates the influence of varying ambient densities on the cone angles of different spray plumes, including plume1–9, plume-thimble, and plume-blocking. The cone angles are illustrated at four times ASOI to provide comparisons. Higher ambient densities result in a larger cone angle during the injection process. In the early stages of the process, before 0.40 ms, there are local differences in cone angles between the holes (plumes1–9)) due to higher initial spray fluctuations. This variation between holes in the injector is more significant during the early stages of the injection process under both ambient densities ($\rho_{amb} = 14.62$ kg/m^3 and $\rho_{amb} = 27.69$ kg/m^3), respectively. However, this variance becomes minimal in relatively developed sprays, particularly after 0.28 ms of ASOI. Figure 13a, b illustrates the initial changes in cone angles, while Fig. 13c, d depicts the changes at later stages of injection. It is also observed that the angles increase gradually with time under both ambient densities during the development of the initial spray. Beyond 0.40 ms, the cone angle remains largely independent of time in both cases (plumes1–9 and plume-thimble). In the case of plume-blocking, the trend is the opposite, with cone angles being slightly higher in the initial spray and decreasing gradually with time. Unlike plumes1–9 and plume-thimble, the cone angles of plume-blocking are higher at the early injection stage (before milliseconds) under both ambient densities. In all three cases (multi-plume, plume-blocking and plume-thimble), the cone angles under higher chamber density are greater than those under lower density. They have a similar trend throughout the injection process.

Fig. 13 Comparison of cone angles for multi-plume and single plume (blocked nozzle and thimble connections) at different ambient densities

(a) 0.171 ms ASOI

(b) 0.286 ms ASOI

(c) 0.40 ms ASOI

(d) 0.543 ms ASOI
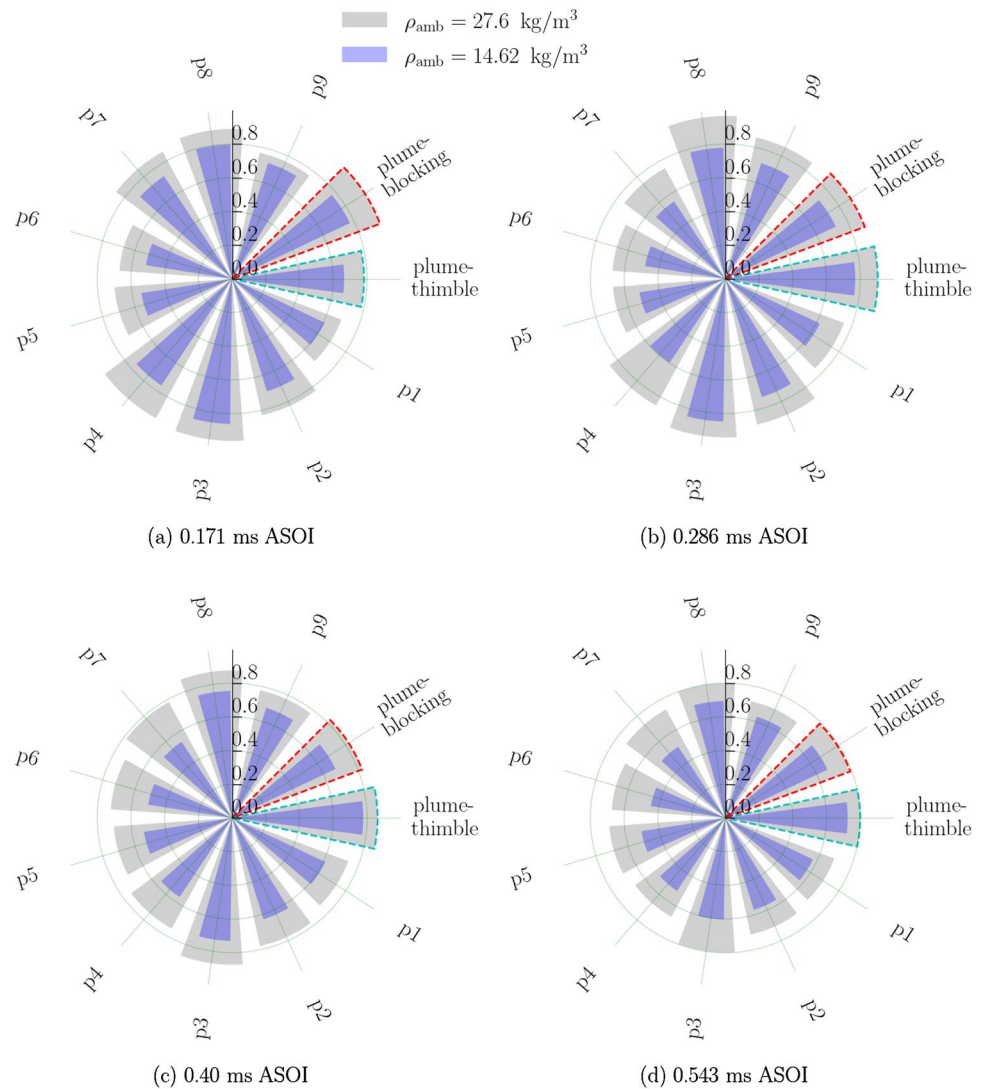
The spray area (SA) is important in determining how fuel is dispersed in the spray field. As depicted in Fig. 14, SA between two ambient densities at one injection pressure (210 MPa) was compared. The results showed no significant difference between the multi-plume and plume-thimble in terms of SA. The plume-blocking approach stood out, displaying a significantly higher SA. This is further evidenced that the thimble approach is a more effective for analysing single sprays than the blocking approach.

4 Summary and conclusions

The article discusses the results of an experiment that aimed to compare and contrast the characteristics of isolated spray plumes (plume-blocking and plume-thimble) and multi-plume from a multi-hole nozzle spray. Based on the results presented in the article, the following conclusions can be drawn:

1. The plume-blocking approach was found to produce greater penetration than all other plume types (plumes1–9) and the plume-thimble. This approach may be less relevant for single-spray analyses due to its rapid penetration, but it also produced smaller cone angles than those fitted with a thimble, which could contribute to its higher penetration levels, because the plume-blocking approach alters the flow distribution within the sac volume and impacts the spray characteristics.

2. When evaluating multi-hole nozzles, deviations in the spray pattern were observed during the early stages of injection. However, over time, this characteristic tended to disappear. Variations in the injection process can occur due to a lack of precision in hole tolerances and lateral needle oscillations.

Fig. 14 Comparison of spray areas for multi-plume and single plume (blocked nozzle and thimble connections) at different ambient densities

(a) 0.171 ms ASOI

(b) 0.286 ms ASOI

(c) 0.40 ms ASOI

(d) 0.543 ms ASOI
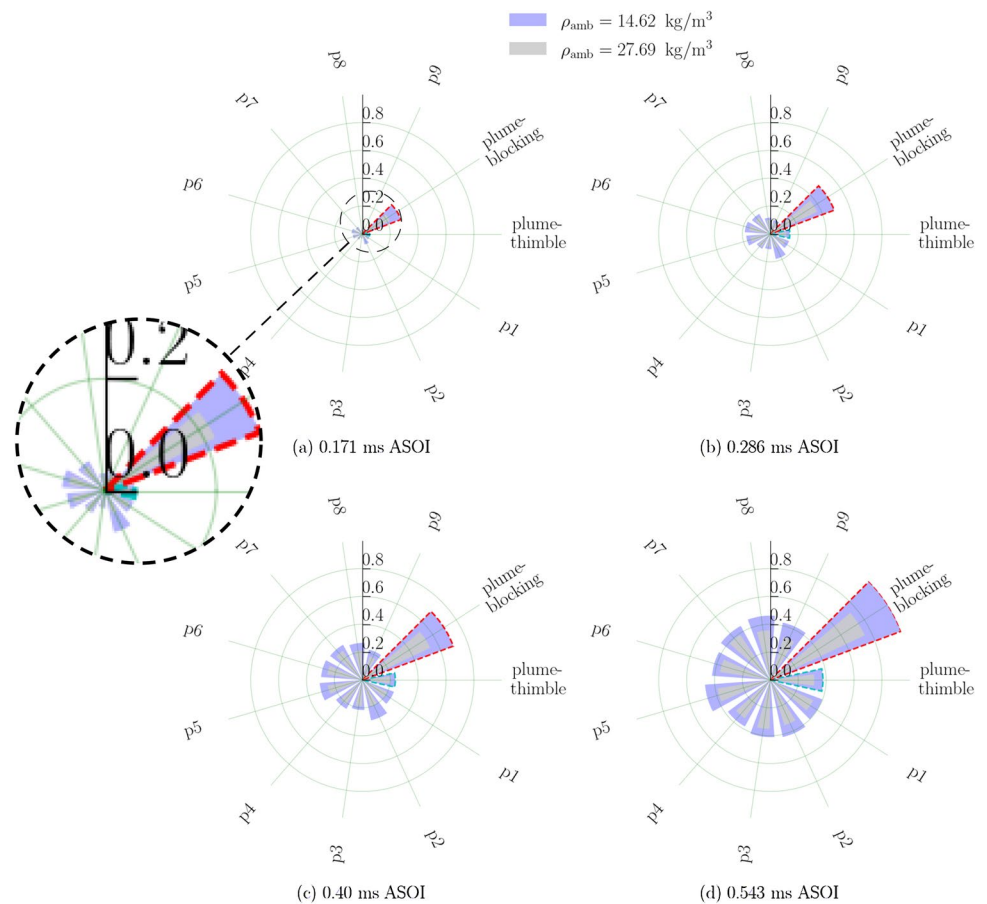
3. Absence of spray interference with the thimble wall was confirmed. Painted inner walls along the thimble depth (Fig. 1b) revealed no erosion during injection. Nevertheless, the intricate design suggests potential benefits, such as enhanced air entrainment, for a thinner wall thickness. However, trade-offs exist, including increased wear and reduced lifespan. A balanced approach, comprehensively evaluating these factors, is essential.

4. The data suggest that shot-to-shot variations in fuel spray from multi-hole nozzles can be attributed to two main factors. Firstly, during transient conditions, the needle movement can be unsymmetrical, particularly at short needle lifts, leading to uneven fuel distribution and plume-to-plume variations upon injection. Secondly, fluctuations in fuel pressure can also contribute to these variations, as changes in pressure can affect the spray pattern, the quantity of fuel delivered, and the velocity of the fuel droplets.

References

Agarwal AK, Gupta T, Shukla PC et al (2015) Particulate emissions from biodiesel fuelled CI engines. Energy Convers Manag 94:311–330. https://doi.org/10.1016/j.enconman.2014.12.094

Baert RS, Frijters PJ, Somers B, et al (2009) Design and operation of a high pressure, high temperature cell for HD diesel spray diagnostics: guidelines and results. https://doi.org/10.4271/2009-01-0649

Battistoni M, Xue Q, Som S et al (2014) Effect of off-axis needle motion on internal nozzle and near exit flow in a multi-hole diesel injector. SAE Int J Fuels Lubric 7:167–182. https://doi.org/10.4271/2014-01-1426

Chandra R, Vijay VK, Subbarao PMV et al (2011) Performance evaluation of a constant speed IC engine on CNG, methane enriched

biogas and biogas. Appl Energy 88:3969–3977. https://doi.org/10.1016/j.apenergy.2011.04.032

Deshmukh D (2011) Studies on atomization and sprays of plant oil biofuels using laser-based diagnostics

He Z, Zhong W, Wang Q et al (2013) Effect of nozzle geometrical and dynamic factors on cavitating and turbulent flow in a diesel multi-hole injector nozzle. Int J Therm Sci 70:132–143. https://doi.org/10.1016/J.IJTHERMALSCI.2013.03.008

Jin Y, Kim J, Kakami S et al (2020) Comparison of diesel spray with small injection amount between single-hole and multi-hole injectors: results under same rail pressure and similar injection rate. Int Commun Heat Mass Transf 118(104):862. https://doi.org/10.1016/J.ICHEATMASSTRANSFER.2020.104862

Klein-Douwel RJ, Frijters PJ, Somers LM et al (2007) Macroscopic diesel fuel spray shadowgraphy using high speed digital imaging in a high pressure cell. Fuel. https://doi.org/10.1016/j.fuel.2006.11.039

Leick P, Bartole K (2023) Experimental investigation into the shift of GDI sprays towards nearby walls via the coandă effect using detailed shadow imaging, particle and structure image velocimetry. Exp Fluids 64(8):144

Luo F, Cui H, Dong S (2014) Transient measuring method for injection rate of each nozzle hole based on spray momentum flux. Fuel 125:20–29. https://doi.org/10.1016/j.fuel.2014.02.011

Macian V, Payri R, Garcia A et al (2012) Experimental evaluation of the best approach for diesel spray images segmentation. Exp Tech 36:26–34. https://doi.org/10.1111/j.1747-1567.2011.00730.x

Moon S, Gao Y, Park S et al (2015) Effect of the number and position of nozzle holes on in- and near-nozzle dynamic characteristics of diesel injection. Fuel 150:112–122. https://doi.org/10.1016/j.fuel.2015.01.097

Okajima S, Kumagai S (1991) Experimental investigation of soot and nox reduction by impinging spray combustion in a closed vessel. Symp Int Combust 23:275–279. https://doi.org/10.1016/S0082-0784(06)80270-5

Otsu N (1979) A threshold selection method from gray-level histograms. IEEE Trans Syst Man Cybern 9(1):62–66. https://doi.org/10.1109/TSMC.1979.4310076

Pal MK, Bhagwat A (2015) Comparison of a single-plume-spray with a multi-plume-spray from a multi-hole common-rail diesel injector. ICLASS 2015, Tainan, Taiwan, August 23–27, p 8

Pal MK, Bakshi S (2017) Study of the effect of ambient vapour concentration on the spray structure of an evaporating n-hexane spray. Exp Thermal Fluid Sci 88:566–575. https://doi.org/10.1016/J.EXPTHERMFLUSCI.2017.07.013

Pal MK, Bakshi S (2018) Effect of ambient fuel vapour concentration on the vapour penetration of evaporating n-hexane sprays. Fuel 223:179–187. https://doi.org/10.1016/j.fuel.2018.02.193

Pastor JV, Arrègle J, García JM et al (2007) Segmentation of diesel spray images with log-likelihood ratio test algorithm for non-gaussian distributions. Appl Opt 46:888. https://doi.org/10.1364/AO.46.000888

Payri R, Gimeno J, Bardi M et al (2013) Study liquid length penetration results obtained with a direct acting piezo electric injector. Appl Energy 106:152–162. https://doi.org/10.1016/J.APENERGY.2013.01.027

Payri R, Gimeno J, Bardi M et al (2013) Study liquid length penetration results obtained with a direct acting piezo electric injector. Appl Energy 106:152–162. https://doi.org/10.1016/j.apenergy.2013.01.027

Payri R, Gimeno J, Viera JP et al (2013) Needle lift profile influence on the vapor phase penetration for a prototype diesel direct acting piezoelectric injector. Fuel 113:257–265. https://doi.org/10.1016/j.fuel.2013.05.057

Payri F, Payri R, Bardi M et al (2014) Engine combustion network: influence of the gas properties on the spray penetration and spreading angle. Exp Thermal Fluid Sci 53:236–243. https://doi.org/10.1016/J.EXPTHERMFLUSCI.2013.12.014

Payri R, Gimeno J, Cuisano J et al (2016) Hydraulic characterization of diesel engine single-hole injectors. Fuel 180:357–366. https://doi.org/10.1016/j.fuel.2016.03.083

Pickett LM, Genzale CL, Bruneaux G et al (2022) Comparison of diesel spray combustion in different high-temperature, high-pressure facilities. SAE Int J Eng 3:27

Pounder CC, Woodyard DF (2004) Pounder's marine diesel engines and gas turbines. In: 8th edn. Elsevier Butterworth Heinemann, oCLC: ocm53231381

Shi J, Lai MC, Zheng Y et al (2011) Characterization of the near-field spray and internal flow of single-hole and multi-hole sac nozzles using phase contrast x-ray imaging and cfd. SAE Int J Eng 4(1):703–719. https://doi.org/10.4271/2011-01-0681

Sombatwong P, Thaiyasuit P, Pianthong K (2013) Effect of pilot fuel quantity on the performance and emission of a dual producer gas-diesel engine. Energy Proc 34:218–227. https://doi.org/10.1016/j.egypro.2013.06.750

Srinivasan KK, Krishnan SR, Qi Y (2014) Cyclic combustion variations in dual fuel partially premixed pilot-ignited natural gas engines. J Energy Resour Technol 136(12):003. https://doi.org/10.1115/1.4024855

Wang C, Moro A, Xue F et al (2018) The influence of eccentric needle movement on internal flow and injection characteristics of a multi-hole diesel nozzle. Int J Heat Mass Transf 117:818–834. https://doi.org/10.1016/j.ijheatmasstransfer.2017.10.057

Wärtsilä Corporation (2023) Wärtsilä: innovative technologies and life-cycle solutions. https://www.wartsila.com. Accessed 02 June 2023

Wei L, Geng P (2016) A review on natural gas/diesel dual fuel combustion, emissions and performance. Fuel Process Technol 142:264–278